F-actin Re-organization Mediates Hierarchical Morphogenesis of Swallowtail Butterfly Wing Scale Nanostructures

Kwi Shan Seah[1,2] and Vinodkumar Saranathan*[1-4]

Affiliations:

[1]Division of Science, Yale-NUS College, 10 College Avenue West, 138609, Singapore.

[2]Department of Biological Sciences, National University of Singapore, 117543, Singapore.

[3]NUS Nanoscience and Nanotechnology Initiative (NUSNNI-NanoCore), National University of Singapore, 117581, Singapore.

[4]Lee Kong Chian Natural History Museum, National University of Singapore, 117377, Singapore.

*E-mail: Vinodkumar.Saranathan@aya.yale.edu

Orcid ID: 0000-0003-4058-5093

Classification: Biological Sciences – Developmental Biology, Cell Biology

Abstract (230 words):

The development of color patterning in lepidopteran wings is of fundamental interest in evolution and developmental biology. While significant advances have recently been made in unravelling the cell and molecular basis of lepidopteran pigmentary coloration, the morphogenesis of wing scales, often involved in structural color

production, is not well understood. Contemporary research focuses almost exclusively on a few nymphalid model taxa (*e.g.*, *Bicyclus*, *Heliconius*), despite an overwhelming diversity across lepidopteran families in the hierarchical nanostructural organization of the scale. Here, we present a time-resolved, comparative developmental study of hierarchical wing scale nanostructure in *Parides eurimedes* and other papilionid species. Our results uphold the putative conserved role of F-actin bundles in acting as spacers between developing ridges as previously documented in several nymphalid species. While ridges are developing, the plasma membrane manifests irregular crossribs, characteristic of Papilionidae, which delineate the accretion of cuticle into rows of planar disks in between ridges. Once ridges have grown, Arp2/3 appears to re-organize disintegrating F-actin bundles into a reticulate network that supports the extrusion of the membrane underlying the disks into honeycomb-like tubular lattices of air pores in cuticle. Our results uncover a previously undocumented role for F-actin in the morphogenesis of wing scale nanostructures prominently found in Papilionidae. They are also relevant to current challenges in engineering of mesophases, since understanding the diversity and biological basis of hierarchical morphogenesis may offer facile, biomimetic solutions.

Key Words: Butterfly Scale, Biological Nanostructure, Hierarchical Morphogenesis, Structural Coloration, Actin Re-organization, Plasma Membrane Invagination

Introduction

The patterning and coloration of butterfly wings have been a paradigmatic focus of extensive research in evolutionary as well as developmental biology due to their fundamental role in signalling and crypsis(1-3). Significant advances have been made recently in identifying the cellular and molecular basis of lepidopteran pigmentary coloration(4-8). A small number of master regulatory genes have been found to exert significant influence on the synthesis and spatial expression of pigments, as well as spatially regulating cuticle deposition thereby affecting the overall scale morphology (e.g., (7)). For instance, suppression of *optix* has been found to tune the thickness of the scale cell's basal surface or lower lamina, inducing iridescent structural coloration(9, 10). Building on the classic studies on cellular organization of lepidopteran scales(11-15), a few recent studies have utilized advances in light microscopy and immunofluorescence to interrogate the formation of longitudinal ridges on the scale's upper lamina(16, 17). These insights are, however, limited to structuring on the scale surface. Moreover, contemporary research on scale cell development(1, 2, 4, 6, 7, 9, 10, 16-18) focuses on a few model taxa (*Bicyclus*, *Precis*, *Heliconius*, *Vanessa*) in one family of butterflies (Nymphalidae), despite an overwhelming diversity in the hierarchical organization of scale nanostructures across Lepidoptera(14, 15, 19, 20). Deciphering the cellular and developmental basis of hierarchical scale cell organization is also highly relevant to current challenges in the mesoscale synthesis of complex hierarchical nanostructures, and could further inspire novel biomimetic routes to fabricate multi-functional materials(21-24).

The *bauplan* of lepidopteran wing scales consist of an ornamented upper lamina over a relatively unstructured basal lamina, supported by arches with pillar-

like struts called trabeculae(19) (Fig. S1R). The upper lamina is essentially a mesh grating, comprising of longitudinal ridges with transverse crossribs framing a set of rectilinear windows. These windows typically open into the interior lumen of the scale cell, but can also be covered by a thin layer of cuticular lamina(19). The sides of the ridges feature microribs – fine flute-like stripes visible at higher magnifications under a scanning electron microscope. The family of swallowtail butterflies (Papilionidae) not only encompasses the known diversity of lepidopteran scale nanostructure, but also exhibits some of the most complex hierarchical mesoscale morphologies found in nature, ranging in size from sub-micron to a few microns(14, 15, 19, 20, 25) (Figs. 1, and S1). In particular, the wing scales of papilionid species (*e.g.*, *Parides arcas, Parides eurimedes*, *Papilio nireus*) exhibit irregular crossribs, often with an underlying honeycomb-like lattice of sheer cuticular walls enclosing columnar pores (hereafter honeycombs), instead of the typical planar, rectilinear crossribs(14, 15, 19, 20, 25) (Fig. 1, and S1).

Here, we use scanning electron microscopy (SEM), confocal microscopy and super-resolution Structured Illumination Microscopy (3D-SIM) to study the time-resolved development of hierarchical scale nanostructure in papilionid wing scales, chiefly in *Parides eurimedes*. Early in development, F-actin bundles act as spacers between developing ridges as previously documented in several nymphalid species(12, 16-18). We further decipher the morphogenesis of the honeycomb lattice conspicuously present in papilionid wing scales. While the ridges are developing, the plasma membrane shows anastomosing, vein-like surface features (crossribs), which appear to delineate the deposition of cuticle into planar disks organized in distinct rows in between the ridges. Mid-development, F-actin bundles that typically disintegrate in nymphalid species once the ridges have grown(16, 17), subsequently

appear to be re-organized by Arp2/3 into a reticulate, mesh-like network that underlies and supports the cuticular disks, as they extrude into the lumen to form the walls of the porous honeycomb lattice. Our findings uncover a previously undocumented role for F-actin in hierarchical butterfly scale cell morphogenesis.

Results

Early stages of scale cell development are conserved in Papilionidae

Early stages of scale cell growth in *P. eurimedes* are as previously documented in wing scales of nymphalid species(12, 16-18). The lectin, wheat germ agglutinin (WGA), fuzzily stains the plasma membrane during early stages of scale development(16). Scale cells from relatively young pupae at 38% development, corresponding to 8 days after pupal formation (APF), resemble elongated buds containing densely packed polymerizing F-actin filaments (Figs. S2A-A'', and B-B''). At 43% development (9 days APF), F-actin filaments form thicker bundles that extend down the full length of scale cells, laying down a scaffold that determines the eventual position of the ridges. WGA stains pleating membranes (longitudinal striations) in between adjacent rows of F-actin bundles (Fig. S2C-C''). Around 48% development (10 days APF), the developing ridges can be more clearly discerned in between F-actin bundles (Figs. S2E-E'', and F-F''). At this stage, there also appears to be irregular gaps in WGA staining in between the ridges, with WGA weakly staining planar, anastomosing vein-like features corresponding to the irregular crossribs seen in adult wing scales (Fig. 1B-C).

Cross-rib and cuticular disk formation

We used lectin and cell membrane stainings to follow cuticle deposition and the plasma membrane topology during scale cell maturation (Figs. 2, and S3-S6). At 48% development (10 days APF), the plasma membrane appears mottled, perhaps showing the beginning of crossrib formation, while WGA predominantly stains sclerotizing longitudinal striations that will become ridges (Figs. 2A-C, and S3B-B''). However, in cross-sections, the two stains appear to co-localize at the periphery of the cell, with plasma membrane underlying the cuticle (Figs. 2C and S3C-C''). This is expected, as the cuticle of extra-cellular origin is deposited on the scale cell membrane.

At 52% pupal development (11 days APF), the plasma membrane shows distinct pleating corresponding to the developing ridges, with the irregular crossribs in between (Figs. 2A'-C', and S4A'-C'). The bulk of the cuticle stained by WGA is restricted to regions in between the membraneous ridges (Figs. 2A'-C', and S4). At around 62% pupal development (13 days APF), the ridges appear to have grown to their near final configuration, while lectin staining reveals planar, disk or droplet-like cuticular features (hereafter cuticular disks) arranged in rows in between the ridges (Figs. 2A''-C'', 2A'''-C''', S5 and S6)

Dynamics of F-actin re-organization

At 57% pupal development (12 days APF), WGA stains cuticular disks of variable sizes observed in a cornrow-like arrangement along the upper lamina, in between where ridges will form (Fig. 3A-C, S7 and movie S1). At this stage, F-actin bundles are breaking down into short fibrils that are distributed around the disks. As the scale cells get more sclerotized and flatten out at 67% development (14 days APF), the disintegrating F-actin can be seen to re-organize and associate more clearly with the

disks, which now appear elongated and slightly tubular in cross-section(Figs. 3A'-C', S8 and movie S2). Most of the linear F-actin bundles have disintegrated at this stage. By 76% development (16 days APF), the disintegrated F-actin bundles re-organize to form distinct tulip bulb-like structures that surround hollow tubular structures comprised of cuticle, *i.e.*, the honeycombs (Figs. 3A''-C'', S9 and movie S3).

In order to better understand the mechanism behind F-actin re-organization (seen in Fig. 3), we tested whether the actin related proteins, Arp2/3 complex, could be directing the dendritic growth of actin fibrils(26, 27) once the bundles disintegrate. At around 11 days APF (Figs. 4A-C, and S10), Arp2/3 complex appear distally in a sparse punctate pattern while the F-actin bundles are still intact. As F-actin bundles disintegrate and start to re-organize around 13 days APF (Figs. 4A'-C', and S11), a relatively higher density of punctate Arp2/3 is seen in close association with the reticulate F-actin network. At a later stage (~16 days APF), the association between Arp2/3 and F-actin is difficult to interpret given the significant overlap of cuticle autofluorescence that has now red-shifted(16) (Figs. 4A''-C'', S12, and S13). Nevertheless, no distinctive punctate patterns can be discerned, which is expected given that the re-organization of F-actin is nearly complete by this stage (Fig. 3). Overall, this suggests Arp2/3 likely plays a key role in the branched re-assembly of actin fibrils.

Conservation of honeycomb morphogenesis in other papilionid species

We also assayed the development of pupal wing scales of several other papilionid species: *Papilio arcas*, *Papilio nireus, Papilio memnon, and Papilio palinurus* (Fig. 5). Our results show that the development of honeycomb lattice is conserved across Papilionidae. Although we were unable to obtain pupae with clearly marked pupation

dates for these species, we observe similar early stages of honeycomb development as seen in *P. eurimedes*. In *P. arcas*, the cuticular disks either appear in planar rows with the actin bundles beginning to break down and re-organize into a reticulate network (Figs. 5A, and B) or the planar crossribs are visible with linear actin bundles still intact (Figs. 5A', and B') – the latter, also in *P. nireus* (Figs. 5A'', and B'') and *P. memnon* (Figs. 5A''', and B'''). In *P. palinurus*, green forewing cover scales feature large concave depressions in between the ridges, while ground scales from green region and black scales show honeycomb lattices typical of Papilionidae (Fig. S1L). Phalloidin staining of pupal *P. palinurus* green cover scales reveals re-organization of longitudinal F-actin bundles into a series of whorl-like rings that underlie the cuticle stained by WGA, which closely correspond to the cuticular dimples or depressions (Figs. 5C, D, C', D', and Movie S4). At lower depths, the actin rings are smaller in size and show a foam-like structure.

Discussion

Swallowtail butterflies (Papilionidae) is the sister lineage to all other butterflies(28) and is indeed the showcase family of lepidopterans, as they exhibit some of the most diverse assortment of wing scale nanostructures(14, 20). Papilionid wing scales also characteristically exhibit irregular crossribs and underlying honeycomb-like lattices of tubular air pores with cuticular walls, although the regularity and depth of the honeycombs can vary (Fig. S1). Such features are unlike the regular, planar, rectilinear crossribs of other lepidopteran families (*e.g.*, Fig. S1R). In this study, we extended previous observations that parallel F-actin bundles configure the spacing and position of longitudinal ridges of wing scales(12, 16-18) to Papilionidae, further

supporting the hypothesis that this mechanism is broadly conserved across lepidopterans.

Our findings further revealed that F-actin re-organization and differential cuticle deposition play a predominant and previously unconsidered role in morphogenesis of butterfly wing scales. Once the longitudinal ridges have developed, F-actin bundles, which typically degenerate in nymphalid species(16, 17), subsequently re-organize into a reticulate network. Interestingly, this actin network appears to draw in the membraneous substrate underlying the cuticular disks into a porous honeycomb lattice. Although F-actin is commonly known to form filamentous rod-like structures, non-linear F-actin morphologies as in this study have been observed in other organisms. In diatoms(29), F-actin organizes into an interdigitating mesh-like porous network during development. This actin network defines frustule (cell walls) morphogenesis by providing a template for silica biomineralization at the meso and micro scales. In mammalian cells, transient ring-like F-actin structures are thought to drive autophagosome generation by serving as a scaffold for mitophagy initiation structures. 3D-SIM revealed F-actin partially associating with mitochondria in the form of curved sheets(30), akin to the F-actin structures seen in this study.

We note that the irregular crossribs characteristic of Papilionidae are in place while the ridges are still growing (Fig. 2A'-C'). These crossribs appear to constrain and delineate the deposition of cuticle into planar disks organized in distinct rows, in between the ridges. A close examination of SEM images (Figs. 1B, and S1) reveals that the endpoints of crossribs at the ridge interface are often connected to microribs present on the ridges. Taken together, this suggests that microrib patterning likely precedes crossrib formation on the surface of scale cell membrane. This is supported by the general lack of crossribs in the basal part of the scale (Figs. S1F,

and H) or rudimentary ones in some scales (Fig. S1O). Given their relatively small size and pitch, we are unable to resolve the development of microribs here, which likely requires high-resolution, live-cell STORM/PALM imaging. However, both the periodic stripes (microribs) and quasi-periodic spots (crossribs) are reminiscent of Turing patterns(31, 32), *i.e.*, implying that an activator-inhibitor type mechanism is perhaps involved in their formation. Alternatively, the crossrib pattern could be a result of random nucleation and growth of perforations on the plasma membrane in between ridges (see Figs. S1F, M, and O).

Overall, the dynamics of cuticle deposition into planar disks delineated by irregular honeycombs and the subsequent actin re-organization appears to be conserved across Papilionidae. However, several *Papilio* species (*e.g.*, *palinurus*, *blumei*, *karna*) possess structurally-colored cover scales(14, 20) with widely-spaced and reduced (in both height and number) ridges. These scales have no apparent crossribs, trabeculae or honeycombs. Instead, they have a characteristic inter-ridge lattice of repeating dimples or concave depressions with microribs that runs the length of the scale, and an underlying perforated lamellae in the scale interior (Fig. S1L-M). Our results suggest that the dimpled appearance of cover scales is templated by re-organization of F-actin bundles into an array of whorl-like rings in between ridges. This could represent perhaps an extreme modification of the developmental program behind the formation of the usual papilionid honeycombs. Without crossribs, the pore sizes of honeycombs are likely constrained only by the pitch of the ridges. This is consistent with our observation that the outermost F-actin rings possess dimensions approaching the inter-ridge distance (Fig. 5C). Without the trabeculae, the lumen multilayer fills the entire interior of the scale right up to the shallow dimples.

Interestingly, in archetypal scale cells, the trabeculae extend downwards from the crossribs and form columns of arches in between the ridges(11-15), suggesting they are developmentally connected (Fig. S1R). Recently, (7) found that *DDC* mutant of *Bicyclus anynana* (Nymphalidae) possessed irregularly-spaced and thin crossribs with sheer, sheet-like vertical trabeculae instead of feet-like, arched trabeculae (see Fig. 4A of (7)). These mutant scale morphologies are somewhat reminiscent of the irregular crossribs and honeycombs of Papilionidae. This suggests spatio-temporal changes in expression patterns of a single gene such as *DDC* could possibly drive honeycomb formation. However, any putative pleiotropic role of pigment-pathway genes in organizing papilionid scale morphology has to be reconciled with that of actin. Future studies could look at pharmacologically-disrupting activity of *DDC* and other pigment-pathway genes during papilionid pupal development, in addition to inhibiting the Arp2/3 complex and tinkering with master regulatory genes like *optix*(9, 10).

The smooth endoplasmic reticulum (SER) has been implicated in templating luminal scale nanostructures during pupal development(15, 25). Given that the papilionid honeycomb lattice extends into the lumen of the scale cells, any putative role of the SER in honeycomb morphogenesis should also be investigated. It would be of interest to follow the development of pupal wing scales using tissue clearing techniques or attempt a more finely resolved developmental time series to capture the full complexity of molecular and cytoskeletal dynamics. Comparatively understanding the diversity and hierarchical nature of biological morphogenesis at the mesoscale could inspire facile, biomimetic routes to synthesizing hierarchically-structured materials for multi-functional applications(21-24).

Materials and Methods

Experimental design

To understand the process of scale nanostructure formation, we performed time-resolved imaging on developing pupal scales using specific biomarkers conjugated with fluorophores. Since cellular membranes and cytoskeletal elements have been identified as key components driving scale cell development, we used biomarkers targeting F-actin, cuticle (chitin) and plasma membrane. We used 3D structured illumination microscope (3D-SIM) and lattice SIM in order to try and resolve structures beyond the diffraction limit. We would have preferred to present all confocal and SIM data solely on a single patch, for instance, the green dorsal forewing cover scales of pupal *P. eurimedes*. However, for time points where scales from the targeted green patch were highly crumpled, we addressed this gap with data from adjacent black areas or from homologous yellow dorsal forewing patch on females. The overall consistency of the results validates our approach.

Dissection of pupae and tissue preparation

Pupae were purchased in multiple batches from Marl Insect and Butterfly Culture (Philippines), Stratford-upon-Avon Butterfly Farm (UK), and Mariposario del Bosque Nuevo (Costa Rica) between June 2017 - June 2020. Precise pupation dates were available only for one batch of *P. eurimedes* pupae. For other *P. eurimedes* batches, we estimate the rough pupation stage (indicated by ~, *e.g.*, Figs. 2A'''-C''', and 4) by morphological comparisons to this batch. Sex of each pupa was determined by examining markings on the ventral segments. Wings from each pupa were dissected in cold Phosphate Buffer Saline (PBS) and immediately fixed in 4% PEM-PFA at

room temperature for 15 mins. Following washes in PBS, wings were placed in blocking buffer (0.5% NP-40) at 4℃ overnight prior to staining.

Developmental time series with Wheat Germ agglutinin, phalloidin and anti-Arp2

Wheat Germ Agglutinin (WGA) was previously used to visualize butterfly scale cell growth and is thought to initially stain plasma membrane before switching to chitin at later developmental stages(16). Phalloidin is a standard method to visualize F-actin. For AF-555 WGA and AF-647 phalloidin double-staining, pupal wings were incubated in 1:200 dilution of Alexa Fluor 555-conjugated WGA (Invitrogen W32464) and 1:40 dilution of Alexa Fluor 647-conjugated phalloidin (Invitrogen A22287) for an hour at room temperature. For FITC WGA and TRITC phalloidin double staining, *P. palinurus* pupal wings were incubated in 1:100 dilution of FITC WGA (EY Labs F-2101-5) and 1:100 dilution of TRITC phalloidin (Sigma P1951) for an hour at room temperature. Arp2 is the ATP-binding component of the actin Arp2/3 complex, which functions as an actin nucleator in branched actin networks. After blocking, pupal wings were incubated with a 1:500 dilution of rabbit anti-Arp2 (Abcam ab47654; pblast search revealed Uniprot #P61160, Human Arp2 has 82% sequence similarity to XP_013178655.1, *Papilio xuthus Arp2*) at 4℃ overnight. After washing, the wings were incubated in buffer with a 1:300 dilution of Alexa Fluor 594 Goat anti Rabbit secondary antibody (Abcam ab150088) for an hour at room temperature.

Time series with CellMask Plasma Membrane stain

As the CellMask plasma membrane stain does not survive permeabilization, dissected pupal wings were immediately stained with a 1:300 dilution of CellMask Deep Red (Invitrogen C10046) for 10 mins. After removing the staining solution, the

wings were fixed in 4% PEM-PFA at room temperature for 15 mins. Following washes in PBS, pupal wings were stained with a 1:200 dilution of Alexa Fluor 555-conjugated WGA (Invitrogen W32464) for an hour at room temperature. In order to prevent permeabilization, the buffers for Cellmask stains did not contain detergents (Triton).

Negative controls

We labelled without primary antibody to determine if the observed fluorescence signal is due to non-specific binding of secondary antibodies. After blocking, pupal wings were incubated without primary antibodies (only buffer) at 4℃ overnight. After washing, the wings were incubated with a 1:300 dilution of Alexa Fluor 594 Goat anti Rabbit secondary antibody (Abcam ab150088) for an hour at room temperature. Negative controls were imaged using the same settings (gain, *etc*.) as the anti-Arp2 antibody stained test samples.

Image acquisition, data processing

Following washes, the wings were mounted on glass slides in Prolong Gold antifade (Life Technologies P36930), covered with #1 thickness coverslips and sealed with nail polish. Confocal images were acquired using Olympus FV3000 (60x), Nikon A1R (100x) and Leica SP8 (100x). 3D-SIM was performed on a DeltaVision OMX and lattice SIM using Zeiss Elyra 7. Confocal data acquired with Olympus FV3000 and Nikon A1RSIM data were deconvolved using default settings in Huygens Professional v20.04. Confocal data acquired with Leica SP8 were deconvolved using default settings in Leica's Lightning deconvolution software during acquisition. All images were examined and processed using Bitplane Imaris Viewer 9.5.1. Movies

were generated using Bitplane Imaris and edited using Shotcut v19.07.15 (Meltytech, LLC)

Scanning electron microscopy (SEM)

Adult scales were individually picked with a needle and placed on carbon tape. Mounted scales were fractured using a razor-blade to obtain cross-sectional views. All samples were sputter-coated with gold to increase conductivity and reduce charging. Samples were imaged using JEOL JSM 6010LV Scanning Electron Microscope at 15-20k. For focused ion beam (FIB) milling, samples were prepared by sputter-coating with platinum to increase conductivity. The sectioned scale shown in Fig. 1C is milled using a gallium ion beam on a FEI Versa 3D with the following settings: beam voltage - 8kV, beam current - 12pA at a 52° tilt. Image acquisition was performed in the same equipment with the following settings: beam voltage - 5kV, beam current - 13pA.

Acknowledgments:

We are indebted to Antonia Monteiro for generously providing us with lab resources, including the use of insectary. We thank Cédric Finet for sharing FIB-SEM image of *P. eurimedes*. We are grateful to A. Monteiro and her lab, C. Finet, Cynthia He, Rong Li, Sasha Bershadsky and Dan Morse for their many thoughtful suggestions. We thank Sree Vaishnavi Sundararajan and Gianluca Grenci (MBI) for access and help with SEM, Tong Yan (CBIS), Mak Kah Jun and Peng Qiwen (MBI), Laura and Keshmarathy Sacadevan (Singhealth Advanced Bioimaging) for help with confocal microscopy, Graham Wright and Goh Wah Ing (A*STAR AMP) and Shi Xianke (Zeiss) for help with SIM data acquisition.

Funding: This work was supported by a Graduate Research Excellence Grant - Rosemary Grant Advanced Award from SSE to K.S., Yale-NUS startup funds (R-607-261-182-121) and a Singapore NRF CRP Award (CRP20-2017-0004) to V.S.

Author Contributions: V.S. and K.S. designed the study. K.S. performed the experiments. Both authors analyzed the results and wrote the manuscript.

Competing interests: Authors declare no competing interests.

References

1. Beldade P & Brakefield PM (2002) The genetics and evo-devo of butterfly wing patterns. *Nat Rev Genet* 3(6):442-452.
2. Sweeney A, Jiggins C, & Johnsen S (2003) Insect communication: Polarized light as a butterfly mating signal. *Nature* 423(6935):31-32.
3. Tsai CC*, et al.* (2020) Physical and behavioral adaptations to prevent overheating of the living wings of butterflies. *Nature communications* 11(1):551.
4. Reed RD*, et al.* (2011) optix Drives the Repeated Convergent Evolution of Butterfly Wing Pattern Mimicry. *Science* 333(6046):1137-1141.
5. Nishikawa H*, et al.* (2015) A genetic mechanism for female-limited Batesian mimicry in Papilio butterfly. *Nature genetics* 47(4):405-409.
6. Nadeau NJ*, et al.* (2016) The gene cortex controls mimicry and crypsis in butterflies and moths. *Nature* 534(7605):106-110.

7. Matsuoka Y & Monteiro A (2018) Melanin Pathway Genes Regulate Color and Morphology of Butterfly Wing Scales. *Cell Rep* 24(1):56-65.

8. Zhang L*, et al.* (2017) Genetic Basis of Melanin Pigmentation in Butterfly Wings. *Genetics*.

9. Wasik BR*, et al.* (2014) Artificial selection for structural color on butterfly wings and comparison with natural evolution. *P Natl Acad Sci Usa* 111(33):12109-12114.

10. Zhang L, Mazo-Vargas A, & Reed RD (2017) Single master regulatory gene coordinates the evolution and development of butterfly color and iridescence. *Proc Natl Acad Sci U S A* 114(40):10707-10712.

11. Overton J (1966) MICROTUBULES AND MICROFIBRILS IN MORPHOGENESIS OF THE SCALE CELLS OF EPHESTIA KÜHNIELLA. *Journal of Cell Biology* 29(2):293-305.

12. Ghiradella H (1974) Development of ultraviolet-reflecting butterfly scales: How to make an interference filter. *Journal of Morphology* 142:395-410.

13. Ghiradella H & Radigan W (1976) Development of butterfly scales. II. Struts, lattices and surface tension. *J Morphol* 150(2):279-297.

14. Ghiradella H (1985) Structure and development of iridescent lepidopteran scales: the Papilionidae as a showcase family. *Ann Entomol Soc Am* 78:252-264.

15. Ghiradella H (1989) Structure and development of iridescent butterfly scales: Lattices and laminae. *Journal of Morphology* 202:69-88.

16. Dinwiddie A*, et al.* (2014) Dynamics of F-actin prefigure the structure of butterfly wing scales. *Dev Biol* 392(2):404-418.

17. Day CR, Hanly JJ, Ren A, & Martin A (2019) Sub-micrometer insights into the cytoskeletal dynamics and ultrastructural diversity of butterfly wing scales. *Developmental Dynamics* 248(8):657-670.

18. Pomerantz AF*, et al.* (2020) Developmental, cellular, and biochemical basis of transparency in the glasswing butterfly Greta oto. *bioRxiv*:2020.2007.2002.183590.

19. Ghiradella H (1984) Structure of iridescent lepidopteran scales: Variation on several themes. *Ann. Entomol. Soc. Am.* 77:637-645.

20. Prum RO, Quinn T, & Torres RH (2006) Anatomically diverse butterfly scales all produce structural colours by coherent scattering. *Journal of Experimental Biology* 209:749-765.

21. Potyrailo RA*, et al.* (2007) Morpho butterfly wing scales demonstrate highly selective vapour response. *Nat Photon* 1(2):123-128.

22. Kolle M*, et al.* (2010) Mimicking the colourful wing scale structure of the Papilio blumei butterfly. *Nat Nanotechnol* 5(7):511-515.

23. Siddique RH*, et al.* (2017) Bioinspired phase-separated disordered nanostructures for thin photovoltaic absorbers. *Science Advances* 3:e1700232.

24. Pokroy B, Kang SH, Mahadevan L, & Aizenberg J (2009) Self-organization of a mesoscale bristle into ordered, hierarchical helical assemblies. *Science* 323(5911):237-240.

25. Saranathan V*, et al.* (2010) Structure, function, and self-assembly of single network gyroid (I4(1)32) photonic crystals in butterfly wing scales. *P Natl Acad Sci Usa* 107(26):11676-11681.

26. Pollard TD (2007) Regulation of Actin Filament Assembly by Arp2/3 Complex and Formins. *Annual Review of Biophysics and Biomolecular Structure* 36(1):451-477.

27. Rouiller I*, et al.* (2008) The structural basis of actin filament branching by the Arp2/3 complex. *Journal of Cell Biology* 180(5):887-895.

28. Espeland M*, et al.* (2018) A Comprehensive and Dated Phylogenomic Analysis of Butterflies. *Curr Biol* 28(5):770-778.e775.

29. Tesson B & Hildebrand M (2010) Extensive and Intimate Association of the Cytoskeleton with Forming Silica in Diatoms: Control over Patterning on the Meso- and Micro-Scale. *PloS one* 5(12):e14300.

30. Hsieh C-W & Yang WY (2019) Omegasome-proximal PtdIns(4,5)P2 couples F-actin mediated mitoaggregate disassembly with autophagosome formation during mitophagy. *Nature communications* 10(1):969.

31. Turing AM (1952) The chemical basis of morphogenesis. *Philosophical Transactions of the Royal Society of London* 237:37-72.

32. Meinhardt H (1982) *Models of Biological Pattern Formation* (Academic Press, London).

Figure 1. Hierarchical nanostructuring of wing scales in *Parides eurimedes* (Papilionidae). (A) Adult male with structurally-colored green patches on their dorsal forewings. Credit: iDigBio YPM Ent 433579 (by CC-1.0). (B) SEM top-view and (C) FIB-SEM cross-sectional image of an adult green scale showing ridges, irregular crossribs and columnar honeycombs ending in wispy trabeculae on top of a perforated multilayer lattice. Scale bars: (A) – 1cm, (B and C) – 1µm.

Figure 2. Morphogenetic time-series of cuticular disks in distinct rows in between ridges in pupal *P. eurimedes* dorsal fore-wing scales acquired with a 100x confocal microscope. Scales are stained with AF-555 WGA (green) and Cellmask (red). By 11 days APF, Cellmask staining reveals hollow anastomosing vein-like crossribs on the plasma membrane in between ridges that serve as boundaries for cuticle accretion. As scales mature, more cuticle is deposited on these rows of disks bounded by membraneous crossribs as compared to the rest of the scale cell surface. See also Figs. S3-S6. (B-B''') Close up views of A-A'''. (C-C''') *xz* cross-sections of the scale at locations marked with grey lines in A-A''' reveal the planar aspect of the cuticular disks, for the honeycomb lattice has not formed yet. Yellow ROI in C'-C''' correspond to those in B'-B'''. Scale bars (A-A''') – 5µm, (B-B''' and C-C''') – 2µm.

Figure 3. Morphogenetic time-series of the development of columnar honeycomb lattice in pupal *P. eurimedes* dorsal fore-wing scale cells acquired with super-resolution lattice SIM. Scales stained with AF-555 WGA (green) and AF-647 phalloidin (red) show a gradual evolution of the cuticular disks from filled-in planar to hollow tubular outgrowths. The disintegrating F-actin bundles show evidence of re-organization from linear to reticulated features with ring-like cross-sections. See also

Figs. S7-S9. (B-B'') Close up views of A-A''. Insets correspond to the regions of interest (ROI) marked in yellow shown with a 3D aspect. (C-C'') *xz* cross-sections of the scale at locations marked with grey lines in A-A''. Scale bars (A-A'') – 5µm, (B-B'', C-C'' and insets) – 1µm.

Figure 4. Arp2/3 is involved in F-actin reorganization in pupal *P. eurimedes* wing scales. Dorsal fore-wing scales stained with AF-594 anti-Arp2 (green) and AF-647 phalloidin (red) acquired with 100x confocal microscope. Initially (~11 days), Arp2/3 complex appear distally in a sparse punctate pattern while the F-actin bundles are still intact. As F-actin bundles disintegrate and re-organize, a relatively higher density of punctate Arp2/3 is seen in close association with the reticulate F-actin network. Our oldest timepoint (~16d) has a large amount of cuticle autofluorescence overlapping with the AF594 signal, but the punctate pattern can no longer be discerned. See also Figs. S10-S12. (B-B'') Close up views of A-A''. (C-C'') *xz* cross-sections of the scale at locations marked with grey lines in A-A''. Yellow ROIs correspond to those in B-B''. Scale bars (A-A'') – 5µm, (B-B'' and C-C'') – 2µm.

Figure 5. Conservation of honeycomb lattice development in pupal wing scales of other papilionid species. All pupal dorsal fore-wing scales are stained with AF-555 WGA (green) and AF-647 phalloidin (red), except for (A''', B''', C, C' and D), which show FITC WGA (green) and TRITC phalloidin (red). (A-B) Maximum projected 3D-SIM micrograph of green cover scales of pupal male *P. arcas* featuring planar cuticular disks similar in shape and arrangement to *P. eurimedes*, with actin bundles beginning to disassemble. (A'-B') Maximum projected 3D-SIM micrograph of green cover scales of a different male *P. arcas* pupa showing irregular crossribs flanked by

F-actin bundles that are still intact. (A''-B'') Maximum projected 3D-SIM micrograph of blue cover scales of pupal *P. nireus*, similarly with crossribs and intact linear actin bundles. (A'''-B'''). 100x confocal micrograph of pupal *P. memnon*. (B-B''') *xz* cross-sections of the scales with ROI at locations marked with grey lines in A-A''' respectively. (C and C') 60x confocal micrographs of green cover scales of pupal *P. palinurus* shown at two different z-planes. A whorl-like network of F-actin rings underlie the cuticular dimples. At lower *z*, the actin rings are smaller in size and show a foam-like appearance. (D) *xz* cross-sections of the scales with ROI at locations marked with grey lines in C-C' respectively. Scale bars (A-A''', B-B''') – 1µm, (C-C', D) – 5µm.

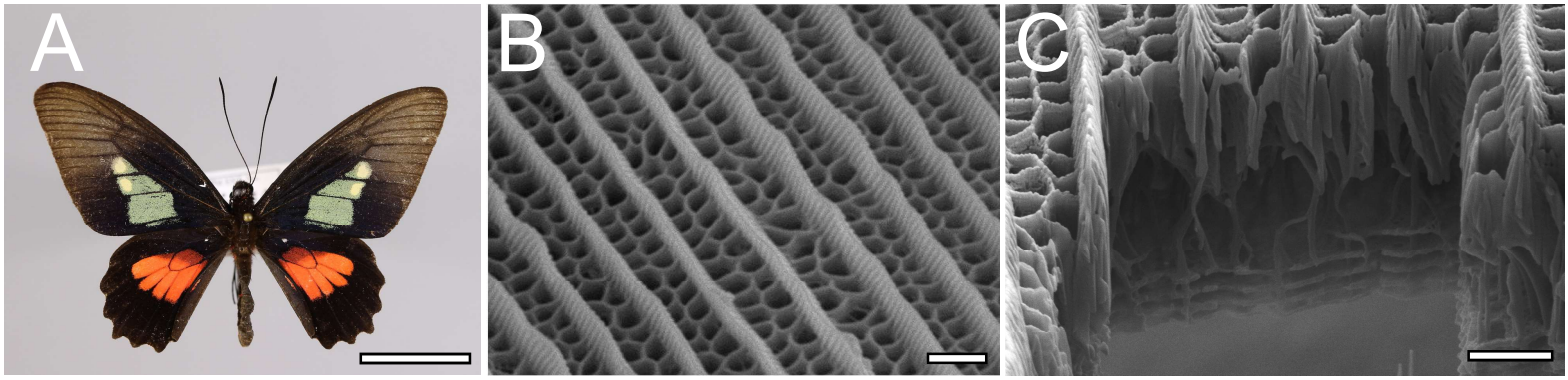
A
B
C

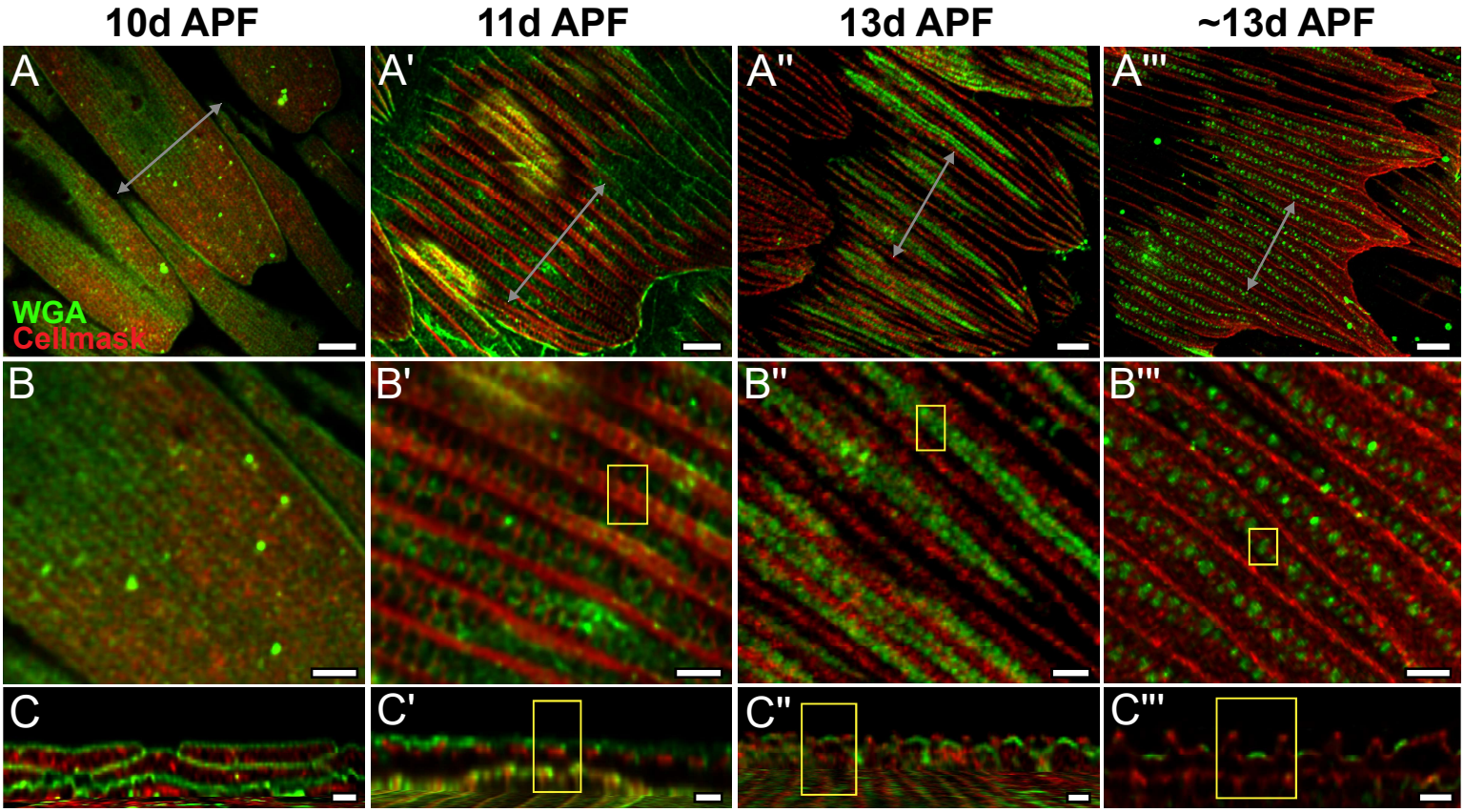
10d APF
11d APF
13d APF
~13d APF
A
A'
A''
A'''
WGA
Cellmask
B
B'
B''
B'''
C
C'
C''
C'''

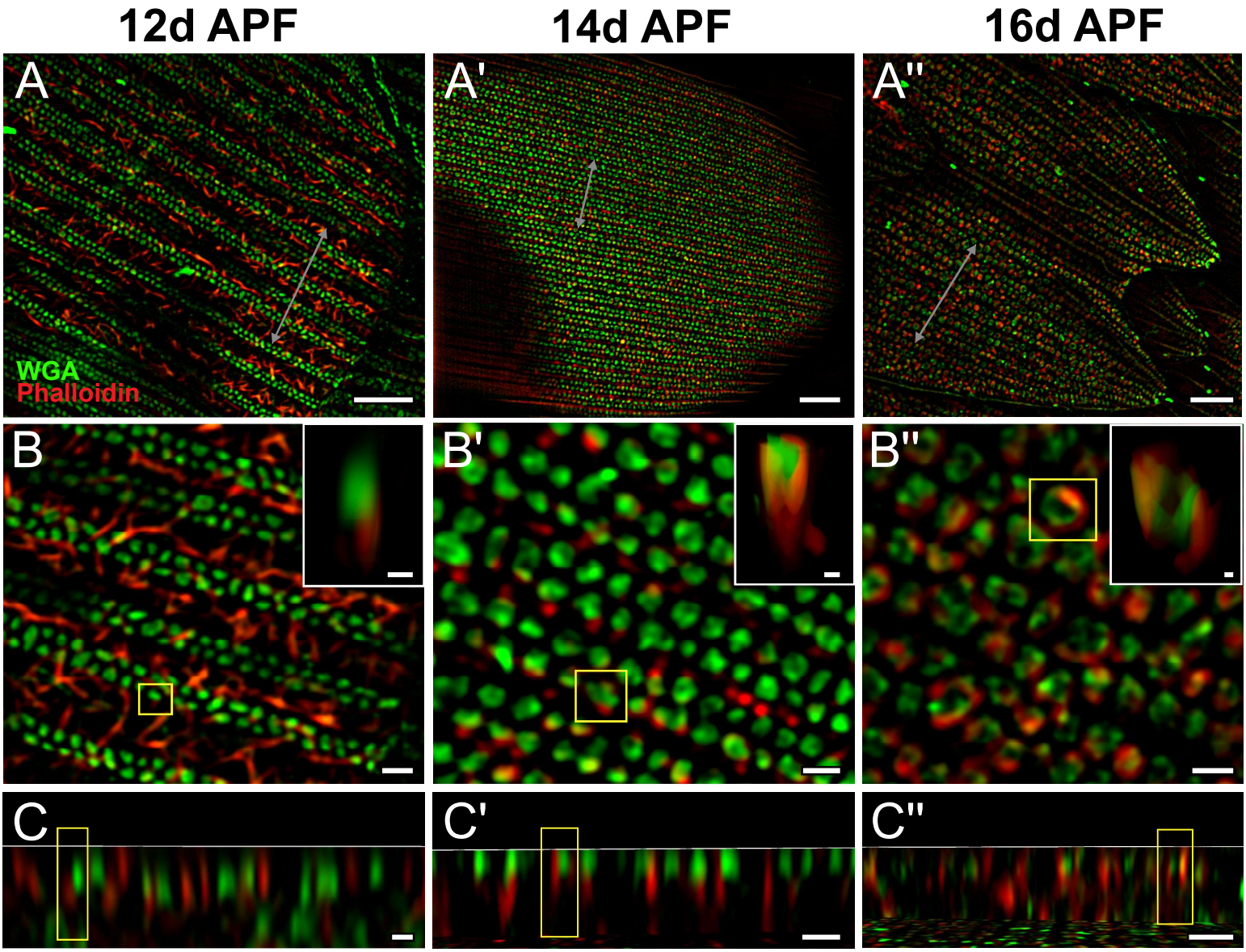
12d APF
14d APF
16d APF
A
A'
A''
WGA
Phalloidin
B
B'
B''
C
C'
C''

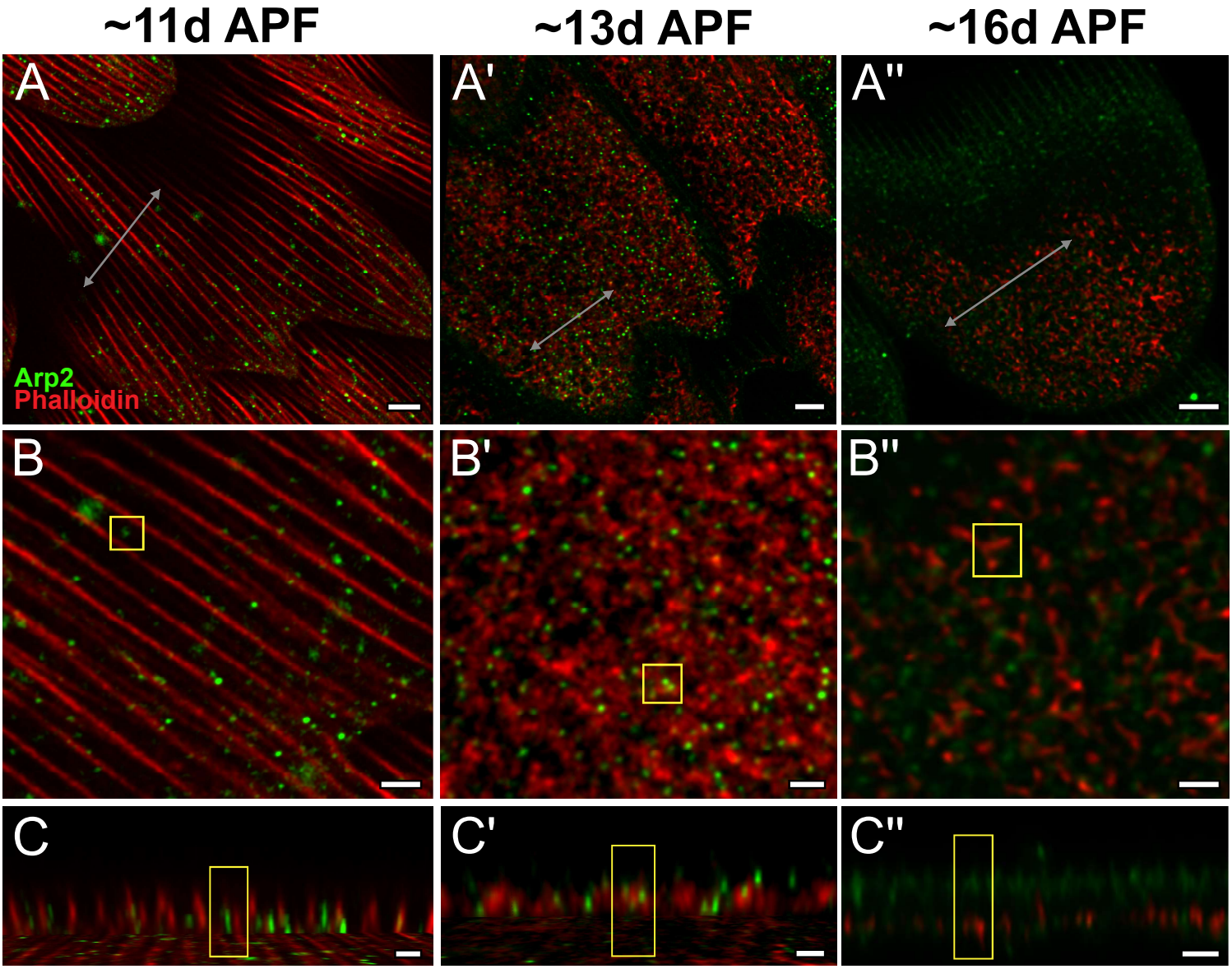
~11d APF
~13d APF
~16d APF
A
A'
A''
Arp2
Phalloidin
B
B'
B''
C
C'
C''

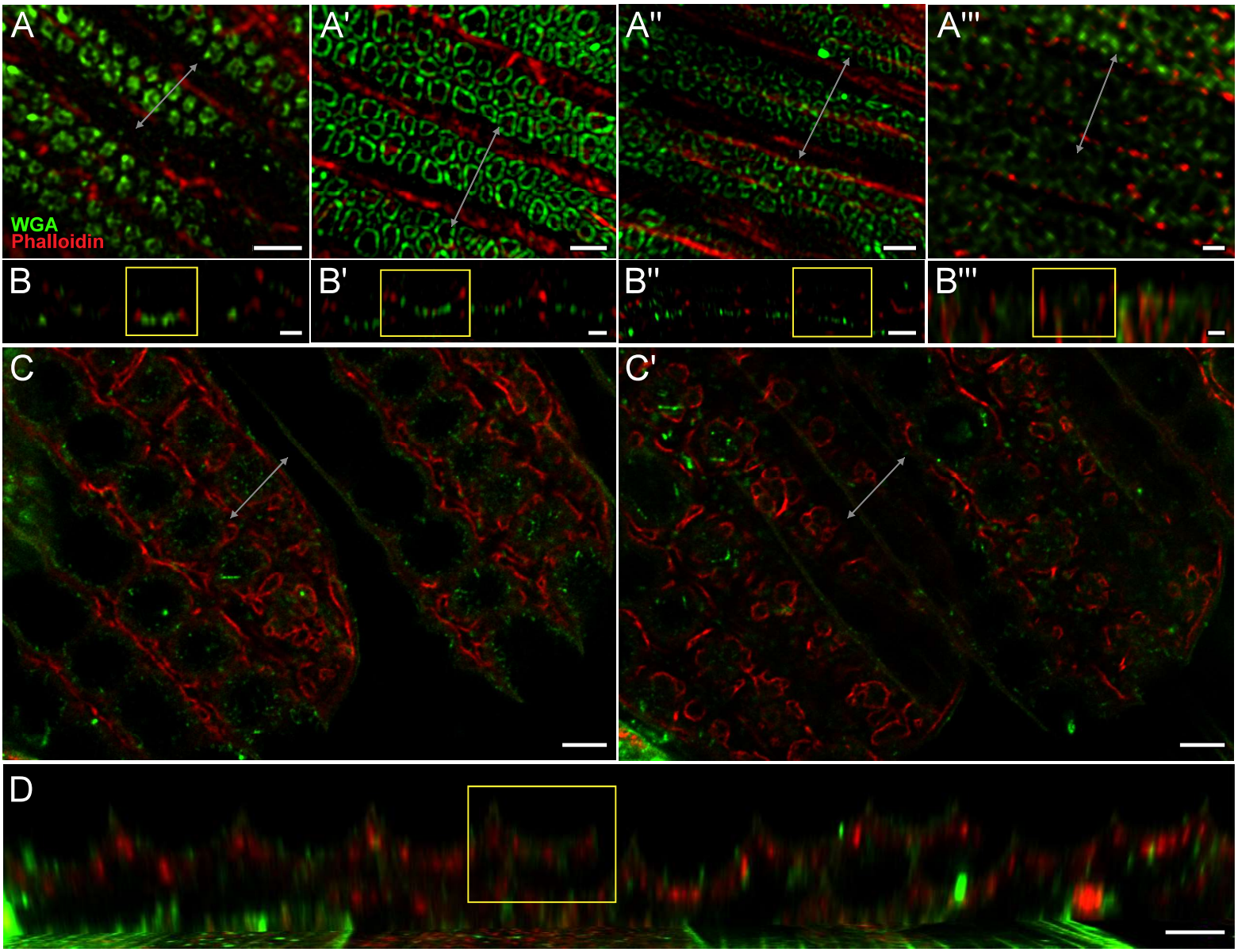
A
A'
A''
A'''
WGA
Phalloidin
B
B'
B''
B'''
C
C'
D